Synthesis, Characterization, and Growth Rates of Germanium Silicalite-1 Grown from Clear Solutions

Chil-Hung Cheng,[§] Gopalakrishnan Juttu,[†] Scott F. Mitchell,[†] and Daniel F. Shantz*[,§]

Department of Chemical Engineering, Texas A&M University, College Station, Texas 77843-3122, and SABIC Technology Center, SABIC Americas, Inc., Sugarland, Texas 77478

Received: June 20, 2006; In Final Form: August 17, 2006

The synthesis, characterization, and growth of Ge-silicalite-1 from optically clear solutions are reported. Ge-silicalite-1 is readily formed from optically clear solutions of TEOS, TPAOH, water, and a germanium source at 368 K. X-ray fluorescence (XRF) is used to determine the Si/Ge ratio and indicates that germanium inclusion is typically 30−50% of that in the actual mixture. Adsorption, power X-ray diffraction (PXRD), and ^{29}Si NMR indicate the materials are crystalline and microporous. In situ small-angle X-ray scattering (SAXS) is applied to investigate the influences of germanium source (GeO_2 and $Ge(OC_2H_5)_4$) and content (Si/Ge 100:5) on the growth of Ge-silicalite-1 from clear solutions at 368 K. The in situ SAXS investigations show that for solutions with Si/Ge ratios of 100, 50, and 25 using $Ge(OC_2H_5)_4$ the induction periods are approximately 6 h and the particle growth rates are 1.82 ± 0.04, 2.52 ± 0.13, and 2.85 ± 0.08 nm/h, respectively, at 368 K, compared to those of pure silicalite-1 (6 h induction period, 1.93 ± 0.1 nm/h growth rate). Further increasing the Si/Ge ratio to 15 and 5 shortens the induction period to approximately 4.5 h, and the growth rates are 3.07 ± 0.16 and 2.05 ± 0.10 nm/h, respectively, indicating the Si/Ge ratio that maximizes Ge-silicalite-1 growth is between 25 and 15. Similar trends are obtained with germanium oxide; however, the growth rates are all consistently larger than those for syntheses with $Ge(OC_2H_5)_4$. The results indicate that Ge-silicalite-1 growth rates in the presence of germanium are increased as compared to those of pure-silica syntheses.

Introduction

Zeolites are crystalline microporous materials which have been widely used in heterogeneous catalysis, the adsorption and separation of gases, and ion-exchange operations.[1−3] Given the importance of these materials to the chemical and petrochemical industries there have been numerous studies of their nucleation and growth. Developing a molecular description of the nucleation/growth process will lead both to new insights about how to design material properties during synthesis as well as suggest new synthesis paradigms for new zeolite phases.[4,5] Silicalite-1, the pure-silica analogue of ZSM-5 (MFI framework topology), has been intensely studied due to the importance of ZSM-5.

From the viewpoint of catalysis the presence of heteroatoms in the framework is essential. Whether it is the ability to introduce extraframework cations (i.e., acid centers) through the presence of trivalent atoms such as aluminum and boron[6−9] or the introduction of redox centers (e.g., Ti^{4+}, Fe^{3+})[7,10−12] in the framework, heteroatom inclusion is essential for catalytic activity. Given the importance of zeolites in catalytic processes the literature is voluminous and will not be reviewed here. However, there is a disconnect between the importance of heteroatom inclusion and the attention it has received in the zeolite nucleation/growth literature. This point motivates the current work.

This disconnect is further highlighted when one compares the numerous studies of silicalite-1 grown from clear solutions.[11,13−33] These works have provided valuable insights into the assembly of silicalite-1 from optically transparent mixtures of TEOS, TPAOH, and water. The only reported study of comparable mixtures containing heteroatoms is work by Cundy's lab on the synthesis of TS-1 from clear solution.[11] That work, while performed at high temperatures (448 K), showed that titanium inclusion in the synthesis mixture leads to a reduction of the growth rate. Finally, from an application vantage, the catalytic properties of zeolites have long been known to depend on the crystal size due to mass transfer effects.[34,35] Given these clear solution syntheses afford small (<200 nm) crystals one may anticipate possible differences in product distributions due to different diffusion path lengths and the potentially increasing importance of reactions on the outer surface of the crystal and other external surface effects.[36−39]

In the current work, the incorporation of germanium into the silicalite-1 structure and how it affects zeolite growth is explored. There are several factors that motivated this choice. First, germanium is the same valence as silicon and as such the framework will remain electrically neutral upon germanium substitution. Second, while many works in the literature have investigated germanium in fluoride-mediated syntheses[40] germanium inclusion in hydroxide-mediated syntheses has not been extensively explored. Third, many reports indicate that the presence of germanium leads to framework topologies possessing a high number of double four-membered rings, implying a structure-directing role for the germanium.[41−49] This observation leads to speculation that germanium may also be preferentially occluded in similar species in solution, something that can potentially be probed by using ^{29}Si solution NMR. These points led us to believe that germanium would be a model heteroatom for investigation. The work below outlines our findings and their

* Address correspondence to this author. Phone: (979) 845-3492. Fax: (979) 845-6446. E-mail: Shantz@che.tamu.edu.
[§] Texas A&M University.
[†] SABIC Americas, Inc.

10.1021/jp063852f CCC: $33.50 © 2006 American Chemical Society
Published on Web 10/03/2006

potential implications for understanding zeolite growth in the presence of heteroatoms.

Experimental Section

Zeolite Synthesis. Ge-silicalite-1 was synthesized from mixtures of composition xTEOS:yGe:0.36TPAOH:20H_2O with $x = 0.990$, 0.980, 0.962, 0.938, and 0.833 and $x + y = 1$. Germanium dioxide (GeO_2, Aldrich, 99.999%) and tetraethoxygermanium ($Ge(OC_2H_5)_4$, Aldrich, 99.95+%) were used as the germanium sources. As an example to prepare Ge-silicalite-1 with Si/Ge ratio = 100, 5 g of TEOS (Fluka, >99.0%) was mixed with 0.0251 g of GeO_2 with stirring for 5 min. 4.44 g of tetrapropylammonium hydroxide (TPAOH, Alfa Aesar, 40 wt % in aqueous solution) was added to the mixture and vigorous stirring was continued for 30 min. Finally, 6.07 g of deionized water was then added and the whole mixture was aged for 24 h at room temperature while mixing. The solution was placed in a screw cap Teflon container and heated at 368 K for 7 days. The solids were collected by centrifugation, washed with deionized water, dried, and characterized by powder XRD. The same solutions were prepared for the in situ SAXS measurements. In the discussion section for clarity the Si/Ge ratios reported in the Results and Discussion are those of the synthesis mixture.

Analytical. Powder X-ray diffraction (PXRD) measurements were performed on a Bruker AXS D8 powder diffractometer (Cu Kα radiation) in reflection mode from $2\theta = 4$ to 50° with a step size of 0.02° and 5 s per step. The PXRD patterns were indexed with the software program PowderX and were refined with Lapod. Field-Emission Scanning Electron Microscopy (FE-SEM) measurements were performed with a Zeiss Leo-1530 microscope operating at 1−10 kV. X-ray fluorescence (XRF) measurements were performed on a Rigaku ZSX100e instrument with a Rh target. The sample was fused with lithium tetraborate before elemental analysis. Nitrogen adsorption experiments were performed on a Micromeritics ASAP 2010 micropore analyzer with a turbo pump capable of obtaining relative pressures of less than 10^{-6}. The samples used in adsorption experiments were first calcined to remove the TPAOH by heating from room temperature to 823 K at a rate of 1 deg/min and were then held at 823 K for 8 h. Samples were degassed at 373 K for 4 h, then at 573 K overnight before performing the measurements. The isotherms were measured over the relative pressure range of 10^{-6} to 0.98. Surface areas and pore volumes were determined by using the α_s method.[50,51]

One-pulse ^{29}Si MAS NMR measurements were performed on a Bruker Avance spectrometer operating at 79.48 MHz. Spectra were acquired by using a 4 mm probe with ZrO_2 rotors, a spinning rate of 5 kHz, a 2 μs 45° pulse, high-power proton decoupling, and a 90 s recycle delay. Chemical shifts were referenced to tetramethylsilane. Solution ^{29}Si NMR spectra were obtained on a Varian Unity Inova 400 MHz spectrometer hosted by a Sun Ultra 5 computer. The samples studied by solution NMR were prepared with isotopically enriched $^{29}SiO_2$ (96+% enriched, Cambridge Isotopes). A Varian 5 mm autoswitchable broadband probe tuned to ^{29}Si (79.38 MHz) was used. The 90° pulse calibration (typically 12 μs) was done on the actual sample. A solution of TMS in $CDCl_3$ as an external reference showed the monomer resonance was at −71 ppm relative to TMS, which was then used as an internal reference.

The in situ SAXS measurements were performed with use of the cell and procedures reported previously.[25,26] All the SAXS experiments were performed on a Bruker NanoSTAR system with a Nonius rotating anode (FR591) and a copper target (1.5417 Å) operating at 45 kV and 90 mA. The precursor solution was loaded in a high-temperature cell and the in situ measurements were performed at 368 K with a measuring period of 1.5 h. Water was used as the reference solvent for background subtraction.

Pair distance distribution functions (PDDFs) were determined from the scattering data by using the program GNOM based on the inverse Fourier transform method (IFT).[52−56] For data during the induction period, the particle diameter was obtained by using the optimized perceptual criteria introduced by Servgun[57] as well as the Guinier approximation.[58] The radius of gyration obtained from the Guinier approximation was calculated by assuming a spherical particle geometry. The values obtained from both approaches were almost identical. For scattering patterns measured following the induction period the particle size distribution was determined to be bimodal in nature. The diameter of the larger particles was determined from the Guinier approximation and the particle diameter of the smaller particles was determined from the optimized perceptual criteria within the smaller guessing value ranges. The theoretical fitting matched the experimental scattering data in the high q range for this optimized guessing value. However, the low q range data could not be described by using just the small particle population. The growth rate during the crystallization period was determined from the particle diameter as a function of the synthesis duration, using linear regression.

Results

Material Characterization. The solid phase collected was identified as silicalite-1 based on PXRD, as shown in Figure 1. No peak splitting was observed in the 2θ range between 22° and 30° upon incorporation of germanium, as displayed in the inset in Figure 1. This along with full pattern indexing indicates all materials are orthorhombic. Given the relatively low germanium incorporation level (see below) of these materials no substantial change in the lattice constants was observed.[59−62] While this result differs from some of the previous work in the literature, it is important to note two important differences between those works and the current report. First, the materials reported here were made in alkaline, not fluoride mediated syntheses (i.e., the pH is higher). Second, the materials reported here have lower germanium contents.

Figure 2 shows the FE-SEM images of samples with a Si/Ge of 25; the FE-SEM images of the other samples can be found in the Supporting Information. Comparing the SEM images of Si/Ge ratio = 100 with that of pure silica silicalite-1 published earlier from our lab,[26] the particle morphology is irregularly spherical and the average diameter is approximately 100 nm. On the basis of the FE-SEM images germanium incorporation, at least at the levels studied here, resulted in no morphological changes as compared to silicalite-1 made under similar conditions. As the germanium content was increased from Si/Ge ratio = 100 to 25, the particle size increased slightly (between 10% and 15%). The particles made in the presence of $Ge(OEt)_4$ were slightly larger than those made in the presence of GeO_2.

Table 1 lists the germanium content of the synthesis mixtures and the as-synthesized samples investigated as determined by XRF. The table shows that for germanium oxide typically 50% (48% for Si/Ge of 100, 53% for Si/Ge of 25) of germanium in the synthesis mixture was incorporated, whereas for syntheses with germanium tetraethoxide the incorporation is approximately 35% (38% for Si/Ge of 100, 30% for Si/Ge of 25). The partial germanium incorporation is consistent with previous literature wherein more efficient germanium incorporation is achieved

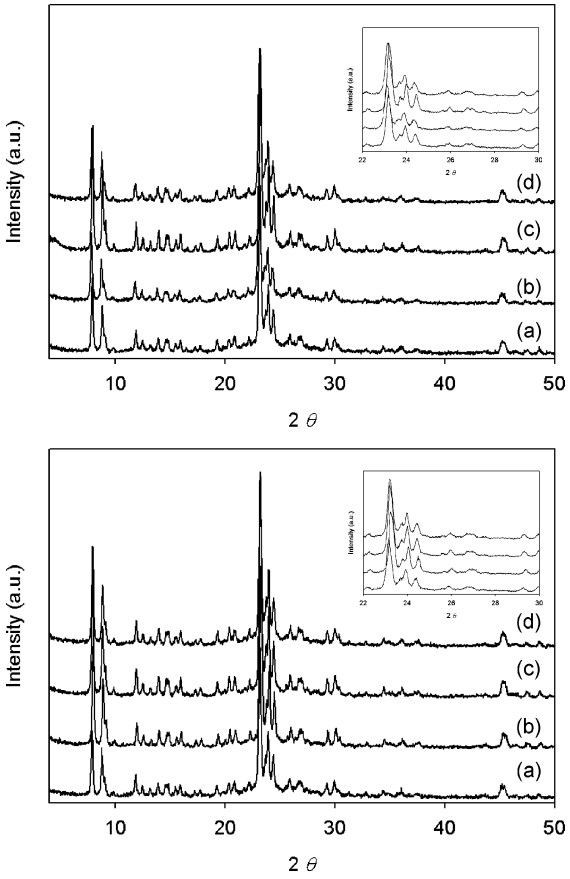

Figure 1. PXRD patterns of Ge-silicalite-1 synthesized from clear solutions at 368 K for 7 days with composition *x*TEOS:*y*Ge:0.36TPAOH:$20H_2O$, where (a) $x = 0.990$ and $y = 0.010$; (b) $x = 0.987$ and $y = 0.013$; (c) $x = 0.980$ and $y = 0.020$; (d) $x = 0.962$ and $y = 0.038$. Ge $= Ge(OC_2H_5)_4$ (top) and GeO_2 (bottom). The inset is the corresponding PXRD patterns magnified showing the 2θ range between 22° and 30°.

via lower pH syntheses and/or fluoride-mediated syntheses.[59,60,63−65] However, on the basis of these results it is possible to incorporate germanium under these conditions.

Figure 3 shows the ^{29}Si MAS NMR spectrum of the calcined sample made with a Si/Ge = 25 and pure silica silicalite-1. Both spectra show a strong signal at −113 ppm assigned to silicon atoms with no Ge atoms as nearest neighbors (Q^4).[59,66] The incorporation of germanium atoms in the MFI framework does not result in a shoulder between −108 and −110 ppm due to Si[1Ge] groups. This is consistent with the XRF results indicating low germanium inclusion (this material has a Si/Ge = 83). However, the broadening of the Q^4 resonance toward upfield observed for the germanium-containing sample is consistent with published results.

The same samples were also characterized by nitrogen adsorption (Figure 4). The micropore volumes are 0.14 and 0.15 cm^3/g for silicalite-1 and Ge-silicalite-1 with a Si/Ge = 25, respectively, showing the germanium-containing materials have micropore volumes comparable to that of the pure silica material. It should also be noted that a substantial amount of nitrogen is adsorbed at higher pressure ($p/p_o > 0.8$). This is also observed for the as-made samples (Supporting Information). The exact origin of this is not clear; however, one possibility is the interstitial void spaces between the zeolite crystals which are ~100 nm in size.[67]

Growth of Ge-Silicalite-1. In situ SAXS measurements were performed to determine how the germanium content and source influence silicalite-1 growth rates. The time-resolved scattering

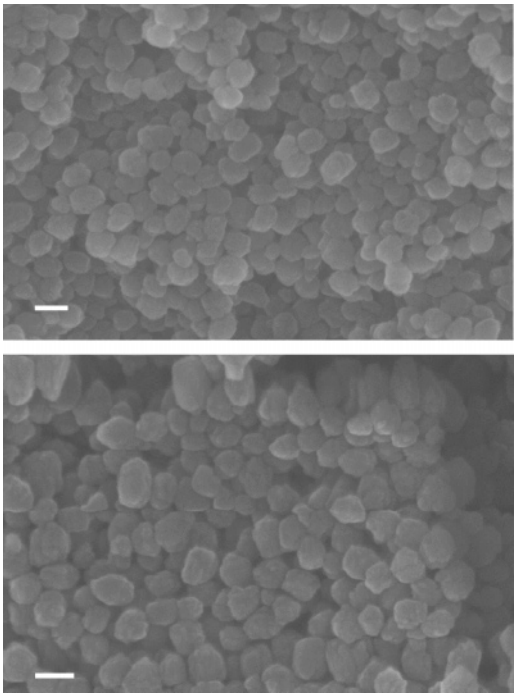

Figure 2. FE-SEM of Ge-silicalite-1 Si/Ge = 25, germanium source (top) GeO_2 and (bottom) $Ge(OC_2H_5)_4$. Scale bar in each image is 100 nm.

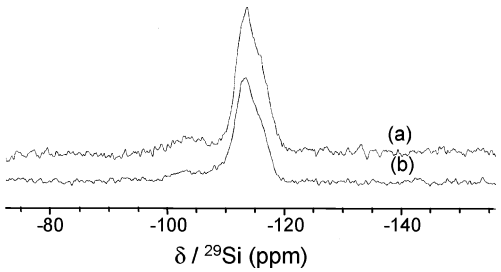

Figure 3. ^{29}Si MAS NMR of (a) silicalite-1 and (b) Ge-silicalite-1 (Si/Ge ratio = 25 with $Ge(OEt)_4$).

TABLE 1: Germanium Content of Ge-Silicalite-1 Samples (XRF)

germanium source	Si/Ge molar ratio of the initial composition	Si/Ge molar ratio of Ge-silicalite-1
GeO_2	100	208
	25	47
$Ge(OC_2H_5)_4$	100	263
	25	83

patterns for the samples made with germanium ethoxide are shown in Figures 5−9 and summarized in Table 2. As has been observed previously for silicalite-1,[14,16,25,29] the particle size distribution of the precursor solution is bimodal in all cases after an induction period due to the appearance of a second particle population whose size is growing during the crystallization period. These particles exist simultaneously with the 4 nm size particles observed during the induction phase.

Figure 5 shows the SAXS patterns of the precursor solution with Si/Ge ratio of 100, using $Ge(OC_2H_5)_4$ as the germanium source. The induction period lasts 4.5−6.0 h, during which the particle diameter remains 4 nm. After the induction period the particles begin to grow based on increasing scattered intensity at low q ranges ($q < 0.05$ $Å^{-1}$). The diameter of the large particles, determined by the Guinier approximation, increases from 4 to 25 nm during the crystallization process, giving a

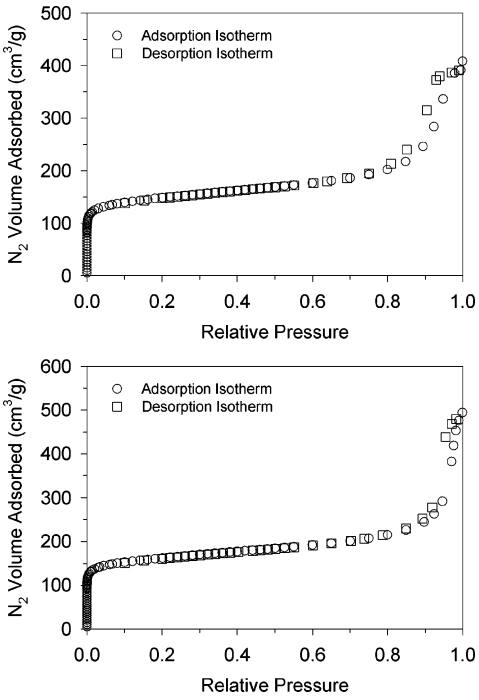

Figure 4. Nitrogen adsorption isotherms of (top) silicalite-1 and (bottom) Ge-silicalite-1 (Si/Ge ratio = 25, $Ge(OEt)_4$).

TABLE 2: Growth Kinetics Summary of Ge-Silicalite-1 from in Situ SAXS Measurements

Ge source	Si/Ge ratio	duration of induction period (h)	appearance of Bragg diffraction peaks (h)	growth rate (nm/h)
GeO_2	100	4.5−6.0	16.5	2.09 ± 0.13
	50	4.5−6.0	13.5	2.81 ± 0.20
	25	4.5−6.0	12.0	3.37 ± 0.14
	15	3.0−4.5	10.5	3.25 ± 0.06
	5	3.0−4.5	13.5	2.50 ± 0.10
$Ge(OC_2H_5)_4$	100	4.5−6.0	16.5	1.82 ± 0.04
	50	4.5−6.0	13.5	2.52 ± 0.13
	25	4.5−6.0	12.0	2.85 ± 0.08
	15	3.0−4.5	10.5	3.07 ± 0.16
	5	3.0−4.5	13.5	2.05 ± 0.10

particle growth rate of 1.82 ± 0.04 nm/h. The slope in the high q range of the scattering patterns is approximately −2.1 and does not change with the synthesis duration, consistent with nonspherical particles. The slope in the high q range of the scattering patterns is independent of the germanium content and source. For this germanium content the induction period becomes shorter and the growth rate is the same within error as for pure silicalite-1 (induction period 6−7.5 h, growth rate 1.93 ± 0.1 nm/h).

Figure 6 shows the time-resolved SAXS data for a Si/Ge ratio of 50 with $Ge(OC_2H_5)_4$ as the germanium source. The induction period is still approximately 4.5−6.0 h, during which the particle diameter remains 4 nm. This is similar to the sample with a Si/Ge ratio of 100. However, Bragg diffraction peaks are now observed after approximately 13.5 h of heating, leading to a particle growth rate of 2.52 ± 0.13 nm/h. This indicates that increasing the germanium content leads to enhanced growth rates. A similar result has been published for ITQ-7;[46] however, this is the first result displaying that a similar effect for germanium is also observed under high pH conditions.

Further increasing the germanium ethoxide content leads to enhanced growth rates as can be observed in Figures 7 and 8. The durations of the induction period are 4.5−6 and 3−4.5 h. The reaction times for the appearance of the Bragg diffraction peaks are further shortened to 12 and 10.5 h leading to growth rates of 2.85 ± 0.08 and 3.07 ± 0.16 nm/h, respectively. Further increasing the germanium ethoxide content (Si/Ge = 5) leads to a reduction in the growth rate to 2.05 ± 0.10 nm/h (Figure 9), which within experimental error is the same as silicalite-1. This result indicates that there is an optimum germanium content if one views the germanium as a promoter for increasing the silicalite-1 growth rate.

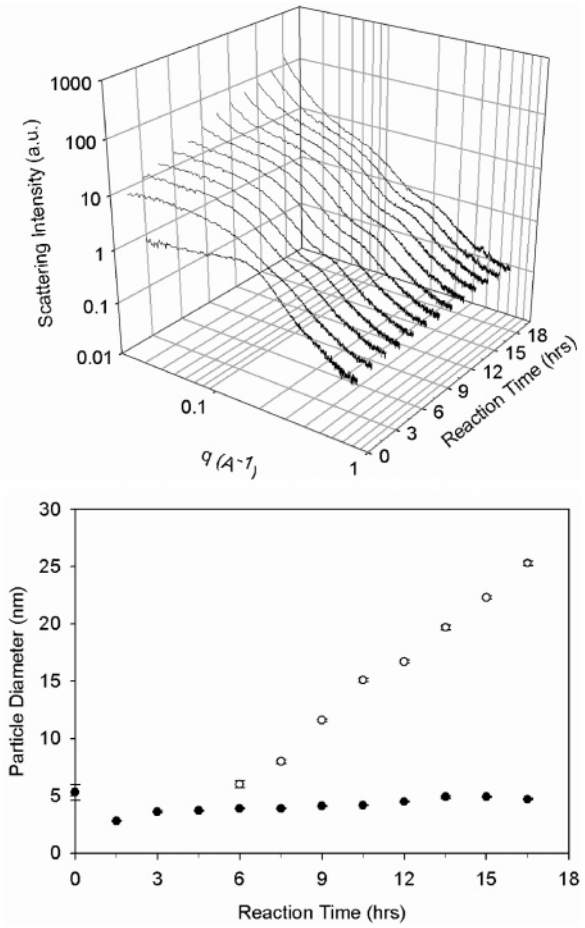

Figure 5. (Top) Time-resolved SAXS scattering patterns of 0.990TEOS: $0.010Ge(OC_2H_5)_4$:0.36TPAOH:$20H_2O$ at 368 K. (Bottom) Plot of particle size versus reaction time.

There are also clear effects upon changing the germanium source from germanium ethoxide to germanium oxide. Figure 10 summarizes the SAXS data showing the growth rate as a function of the synthesis mixture Si/Ge ratio; the figure also includes the same information for silicalite-1. The SAXS data and analysis for the samples made with germanium oxide are shown in the Supporting Information and summarized in Table 2. Again an increase in the growth rate is observed as the Si/Ge ratio decreases, and the maximum growth rate is between a Si/Ge ratio of 25 and 15. This result is similar to those studies while changing the silica source from monomeric to polymeric.[28,29,68] One explanation for this is the higher solubility of germanium oxide/hydroxide species at high pH values as compared to silica.

The work above shows two interesting points. First, the presence of germanium in the synthesis mixture appears to act as a promoter for silicalite-1 growth. Second, the XRF results indicate that a significant portion of the germanium does not incorporate into the growing zeolite framework. One possibility was that the germanium altered the speciation of the mixture. ^{29}Si solution NMR of enriched mixtures containing a Si/Ge =

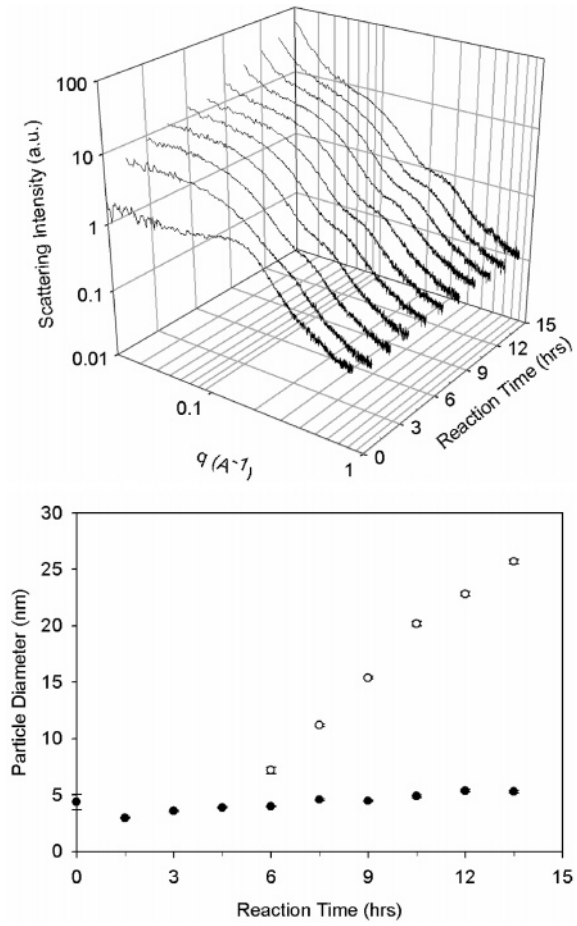

Figure 6. (Top) Time-resolved SAXS scattering patterns of 0.980TEOS: $0.020Ge(OC_2H_5)_4$:0.36TPAOH:$20H_2O$ at 368 K. (Bottom) Plot of particle size versus reaction time.

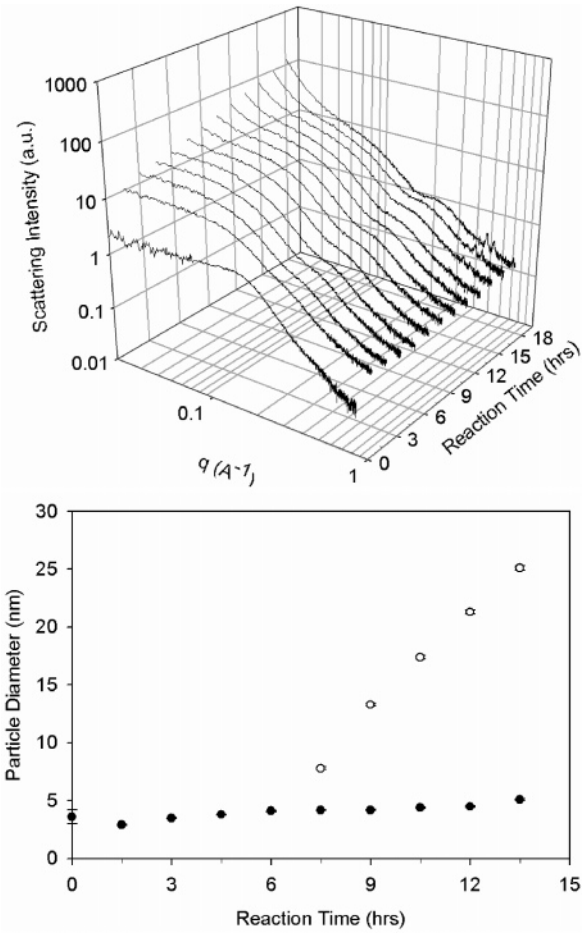

Figure 7. (Top) Time-resolved SAXS scattering patterns of 0.962TEOS: $0.038Ge(OC_2H_5)_4$:0.36TPAOH:$20H_2O$ at 368 K. (Bottom) Plot of particle size versus reaction time.

25 (Supporting Information) indicate that this is not the case as the spectra are almost identical with those of the pure silica solutions (Figure 1 in ref 69) with only slight differences in the relative intensities of the various resonances. Another possibility is the alcohol affecting the growth rate;[26] the syntheses with GeO_2 do contain slightly less ethanol than those with $Ge(OC_2H_5)_4$ but all of these (except for a Si/Ge = 75 ($Ge(OC_2H_5)_4$) have a higher growth rate than that of pure silicalite-1. This leads us to conclude that germanium acts as a promoter for silicalite-1 growth. The explanation for this is at the moment somewhat unclear as is the presence of the maximum of the growth rate at a Si/Ge between 25 and 20. It was hoped that the solution ^{29}Si NMR work would provide some clues but it did not.

Discussion

The results presented above clearly demonstrate the influence of germanium content and source on the growth rate of isomorphous substituted silicalite-1 from clear solutions at 368 K. As summarized in Figure 10 and Table 2 the incorporation of germanium in silicalite-1 precursor solutions leads to larger silicalite-1 growth rates. At higher germanium levels (Si/Ge > 25) a shortening of the induction period is also observed. Given that the SAXS measurements are performed over 90 min intervals the changes in the induction period are close to the time resolution of the measurements, but the results support that increasing the germanium content of the mixture decreases the time period needed to form larger particles (i.e., increases nucleation). The increased growth rates depend on the germanium source used as GeO_2 leads to larger silicalite-1 growth rates than $Ge(OC_2H_5)_4$. Furthermore, this effect becomes more pronounced with the germanium content, with a maximum in the growth rate at Si/Ge ratios between 25 and 15. Thereafter, a decreased silicalite-1 growth rate is observed with further increasing germanium content (lower Si/Ge ratios).

Ideally the SAXS data could be more thoroughly scrutinized to give quantitative information about the number density of particles as has been recently reported by Rimer and co-workers[20] and Davis and co-workers.[31] However, given the strong particle−particle interactions (i.e., $S(q) \neq 1$) as manifested by a clear maximum in the I versus q plots such an analysis does not seem warranted. From a more qualitative vantage, the *relative trend* in the number density of particles can be estimated from the $I(0)$values and are listed in Table 3. No clear trend emerges from these data. For comparison, the $I(0)$ value for pure silicalite-1 is 6.0.[25] This indicates that the number density of the primary particles in the germanium-containing mixtures before heating is lower than in the case of the pure silica mixtures. Calculations were also performed to estimate the relative fraction of primary particles and growing particles when the growing particles were approximately 25 nm in diameter. These results are also summarized in Table 3 and the details of the calculations are given in the Supporting Information. From these results the ratio of primary to growing particles increases with increasing germanium content in the synthesis mixture. This result is consistent with the XRF results that indicate partial incorporation of germanium in the zeolite crystals. Comparing this to the pure silicalite-1 material (data taken from ref 25), the ratio for that mixture is 1.78:1 primary:growing particles.

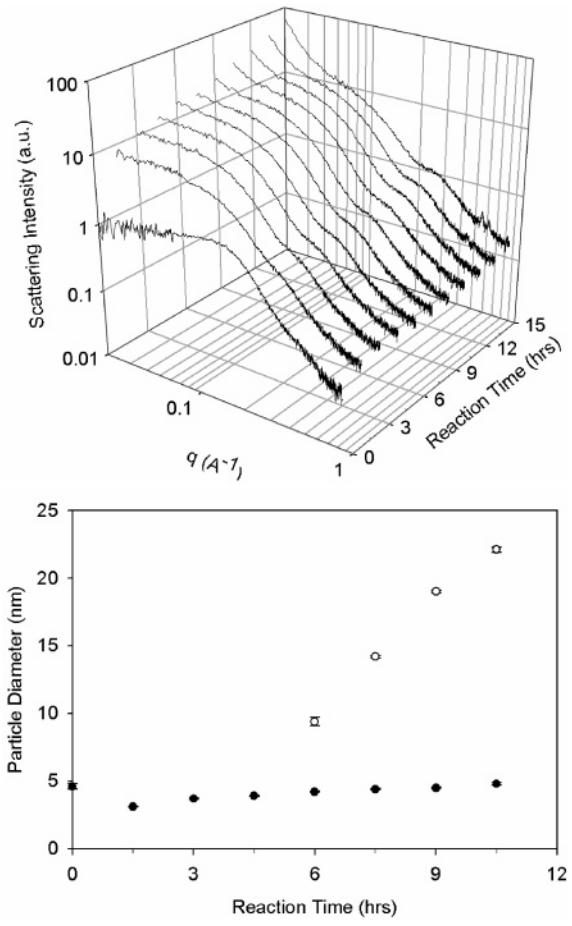

Figure 8. (Top) Time-resolved SAXS scattering patterns of 0.938TEOS: $0.063Ge(OC_2H_5)_4$:0.36TPAOH:$20H_2O$ at 368 K. (Bottom) Plot of particle size versus reaction time.

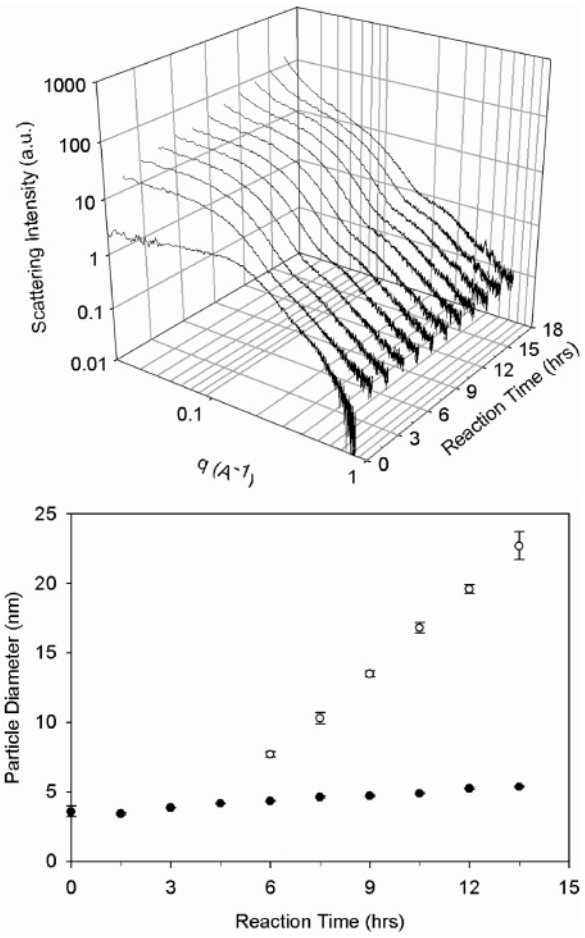

Figure 9. (Top) Time-resolved SAXS scattering patterns 0.833TEOS: $0.167Ge(OC_2H_5)_4$:0.36TPAOH:$20H_2O$ at 368 K. (Bottom) Plot of particle size versus reaction time.

This value is lower than all the values for the germanium-containing mixtures except GeO_2, Si/Ge = 100. Given the assumptions made (e.g., small and large particles have same electron density contrast) it is more appropriate to look at the trends rather than the absolute values.

It is also worthwhile to comment on the current results in the context of numerous recent works on dilute clear solution syntheses of silicalite-1.[19,20,23,31] In agreement with those works as well as many studies of concentrated clear solutions[13,14,18,70] there are small particles present from the initial stages of synthesis. Upon heating a second population of particles is observed that continue to grow throughout the heating period. These particles ultimately become Ge-silicalite-1; at what point they are zeolite was not definitively ascertained here. However, they typically diffract (i.e., unequivocal evidence of zeolite formation) at 20 nm in size. It is certainly possible that these particles possess the silicalite-1 structure before such clear diffraction peaks are observed; however, no methods such as TEM were used here to prove that. One result here in contrast to the work by Davis and co-workers is that the ratio of primary and growing particles is on the order of one. In their report the growing crystals were a very small percentage, approximately 5%, of the total number of particles. Many reasons could account for this difference. The mixtures studied here are much more concentrated, leading to much higher concentrations of silica as well as an increase in the solution pH.[70] Whether or not the larger particles observed in this work form by aggregation of the small primary particles as shown in previous work for dilute silicalite-1 mixtures[31,71] is unknown.

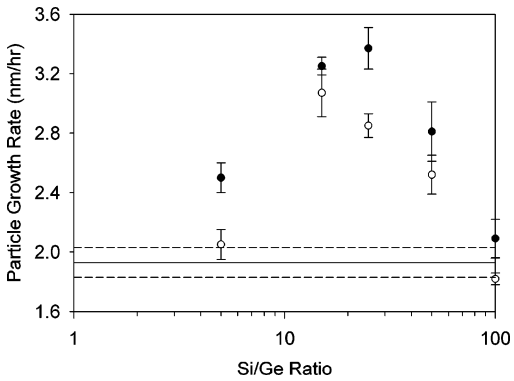

Figure 10. Particle growth rate versus the Si/Ge ratio for Ge-silicalite-1 (solid circles: GeO_2; open circles: $Ge(C_2H_5O)_4$). The solid line is the particle growth rate for TPA-silicalite-1[25] and the dashed lines represent one standard deviation.

From XRF the germanium content of the as-synthesized materials is typically 30−50% that of the precursor solutions. This low germanium incorporation is consistent with published results,[60] and is insensitive to increased synthesis durations, i.e., the same Ge/Si content for Ge-silicalite-1 was observed for a sample synthesized at 368 K for one month. While fluoride-mediated syntheses result in higher germanium inclusion, this is likely a pH effect as those syntheses have pH values below 10 and often closer to 7−8. So while it is tempting to draw comparisons with the fluoride-mediated syntheses it is likely not useful, given the substantially lower pH values, as well as

TABLE 3: Initial Scattered Intensity ($I(0)$) and Estimate of the Ratio of Primary Particles to Growing Crystals from in Situ SAXS Measurements

Ge source	Si/Ge ratio	$I(0)$ before heating	ratio of primary particles to growing crystals[a]
GeO_2	100	3.3	1.33:1 (16.5)
	25	3.5	3.50:1 (15)
$Ge(OC_2H_5)_4$	100	1.9	2.21:1 (16.5)
	25	2.1	3.59:1 (13.5)

[a] Heating duration at 368 K (in hours) given in parentheses. In all cases the growing crystals are approximately 25 nm in diameter.

the differences in fluoride- versus hydroxide-mediated syntheses which have been well documented previously.[72]

The most interesting result is that while the germanium inclusion is incomplete (likely due to pH effects) the germanium shows a clear promotion on zeolite growth. Qualitative analysis of the SAXS data indicates a decrease in the number density of primary particles in the presence of germanium and also indicates an increase in the ratio of primary particles to growing crystals when the growing crystals are approximately 25 nm in size (i.e., zeolite). One of the reasons for obtaining the enhanced zeolite growth rate could be the decrease in the particle number density when germanium atoms are added to replace silicon atoms in the precursor solutions. Persson and co-workers observe a somewhat similar effect when decreasing the TPAOH content and in their case it is likely a pH effect.[28] Furthermore, germanium oxide-containing precursor solutions consistently show higher crystallization rates than those containing $Ge(OC_2H_5)_4$. This promotion effect depends on the germanium content and could be attributed to either the alteration of condensation/dissolution reactions of silicates species or a shift in speciation. The former could be rationalized as germanium oxide is easily ionized at high pH (>12) and becomes a four-coordinated species of $GeO_2(OH)_2^{2-}$, following the reactions[59,60,68]

$$GeO_2 + 2H_2O \leftrightarrow Ge(OH)_4\,(aq)$$

$$Ge(OH)_4\,(aq) \leftrightarrow H^+ + GeO(OH)_3^-$$

$$GeO(OH)_3^- + OH^- \leftrightarrow GeO_2(OH)_2^{2-}$$

The conversion of GeO_2 to $GeO_2(OH)_2^{2-}$ is about 95%, independent of GeO_2 content.[73] However, the second dissolution of silicon is about 30%.[73] This might cause a decrease of pH in the vicinity of Ge atoms, leading to smaller dissolution rates of growing silicalite-1 particles. The second reason is not supported by solution NMR studies performed, although this could be a consequence of the low germanium content of these mixtures. Previous NMR studies of germanium silicate mixtures by Knight and co-workers employed much lower Si/Ge ratios (~1).[74,75] The reason for an optimum Si/Ge ratio is still unclear.

The observed slower silicalite-1 growth rate upon changing GeO_2 to $Ge(OC_2H_5)_4$ as the germanium source could be due to either the excess amount of ethanol content compared with GeO_2 cases or the hydrolysis of tetraethoxygermanium. As published previously, we showed the ethanol content also affects silicalite-1 growth rates. While this may contribute to the observed growth enhancement, the syntheses with $Ge(OC_2H_5)_4$ have the same ethanol content as the pure silica syntheses and consistently have higher growth rates, indicating that the enhancement in growth is due to the germanium, not the (minor) decrease in the ethanol content.

Conclusions

This work quantitatively demonstrates the effect of germanium content and source on the growth of silicalite-1 from optically transparent precursor solution at 368 K by using in situ SAXS technique. All the synthesized silicalite-1 materials show Ge incorporation between 30% and 50%, which is likely a result of the high pH of the synthesis used. The results also show promotion of silicalite-1 growth in the presence of germanium. This enhancement of growth goes through a maximum at Si/Ge between 25 and 15.

Acknowledgment. The authors acknowledge financial support from SABIC Americas Inc. The SAXS instruments were purchased from funds obtained under NSF grant CTS-0215838. The authors acknowledge the X-ray Diffraction Facility at Texas A&M University for access to the XRD and SAXS instruments, Seunguk Yeu for acquiring the FE-SEM images, and Dr. Bakhmoutov and Dr. Sarathy in the Department of Chemistry at Texas A&M University for assistance with the NMR measurements. The solid-state NMR instrument was supported by the National Science Foundation under grant CHE-0234921. The FE-SEM instrument was supported by the National Science Foundation under grant DBI-0116835.

Supporting Information Available: Calculation of the ratio of primary particles to growing crystals from the SAXS data, FE-SEM images of samples, adsorption isotherms of as-made silicalite-1 and calcined silicalite-1 annealed at 1073 K for 12 h, summary of the adsorption data, ^{29}Si solution NMR spectra, FTIR spectrum of the solid collected from the mixtures with composition $0.987TEOS:0.013GeO_2:0.36TPAOH:20H_2O$ and $1TEOS:0.36TPAOH:20H_2O$ performed in a Teflon container at 368 K for 7 days; the time-resolved SAXS patterns and the corresponding evolution of particle size of germanium−silicalite-1 precursor solutions with Si/Ge = 100, 50, 25, 15, and 5, using GeO_2 as the germanium source. This material is available free of charge via the Internet at http://pubs.acs.org.

References and Notes

(1) Barrer, R. M. *Hydrothermal Chemistry of Zeolites*; Academic Press: London, UK, 1982.
(2) Breck, D. W. *Zeolite Molecular Sieves*: *Structure, Chemistry and Use*; Wiley: New York, 1974.
(3) Szostak, R. *Molecular Sieves−Principles of Synthesis and Identification*; Van Nostrand Reinhold: New York, 1989.
(4) Cundy, C. S.; Cox, P. A. *Chem. Rev.* **2003**, *103*, 663−701.
(5) Cundy, C. S.; Cox, P. A. *Microporous Mesoporous Mater.* **2005**, *82*, 1−78.
(6) Tuan, V. A.; Falconer, J. L.; Noble, R. D. *Microporous Mesoporous Mater.* **2000**, *41*, 269−280.
(7) Millini, R.; Perego, G.; Bellussi, G. *Top. Catal.* **1999**, *9*, 13−34.
(8) Jareman, F.; Hedlund, J.; Sterte, J. *Sep. Purif. Technol.* **2003**, *32*, 159−163.
(9) de Ruiter, R.; Jansen, J. C.; van Bekkum, H. *Zeolites* **1992**, *12*, 56−62.
(10) Bordiga, S.; Damin, A.; Bonino, F.; Ricchiardi, G.; Zecchina, A.; Tagliapietra, R.; Lamberti, C. *Phys. Chem. Chem. Phys.* **2003**, *5*, 4390−4393.
(11) Cundy, C. S.; Forrest, J. O.; Plaisted, R. J. *Microporous Mesoporous Mater.* **2003**, *66*, 143−156.
(12) Szostak, R.; Nair, V.; Thomas, T. L. *J. Chem. Soc., Faraday. Trans. 1* **1987**, *83*, 487−494.
(13) Schoeman, B. J.; Sterte, J.; Otterstedt, J. E. *Zeolites* **1994**, *14*, 568−575.
(14) Schoeman, B. J.; Regev, O. *Zeolites* **1996**, *17*, 447−456.
(15) Schoeman, B. J. *Microporous Mesoporous Mater.* **1997**, *9*, 267−271.
(16) Schoeman, B. J. *Zeolites* **1997**, *18*, 97−105.
(17) Schoeman, B. J. *Stud. Surf. Sci. Catal.* **1997**, *105*, 647−654.
(18) Schoeman, B. J. *Microporous Mesoporous Mater.* **1998**, *22*, 9−22.

(19) Rimer, J. D.; Lobo, R. F.; Vlachos, D. G. *Langmuir* **2005**, *21*, 8960−8971.
(20) Rimer, J. D.; Vlachos, D. G.; Lobo, R. F. *J. Phys. Chem. B* **2005**, *109*, 12762−12771.
(21) Nikolakis, V.; Tsapatsis, M.; Vlachos, D. G. *Langmuir* **2003**, *19*, 4619−4626.
(22) Kragten, D. D.; Fedeyko, J. M.; Sawant, K. R.; Rimer, J. D.; Vlachos, D. G.; Lobo, R. F.; Tsapatsis, M. *J. Phys. Chem. B* **2003**, *107*, 10006−10016.
(23) Fedeyko, J. M.; Rimer, J. D.; Lobo, R. F.; Vlachos, D. G. *J. Phys. Chem. B* **2004**, *108*, 12271−12275.
(24) Fedeyko, J. M.; Vlachos, D. G.; Lobo, R. F. *Langmuir* **2005**, *21*, 5197−5206.
(25) Cheng, C.-H.; Shantz, D. F. *J. Phys. Chem. B* **2005**, *109*, 13912−13920.
(26) Cheng, C.-H.; Shantz, D. F. *J. Phys. Chem. B* **2005**, *109*, 19116−19125.
(27) Mintova, S.; Valtchev, V. *Microporous Mesoporous Mater.* **2002**, *55*, 171−179.
(28) Persson, A. E.; Schoeman, B. J.; Sterte, J.; Ottesstedt, J. E. *Zeolites* **1994**, *14*, 557−567.
(29) Watson, J. N.; Iton, L. E.; Keir, R. I.; Thomas, J. C.; Dowling, T. L.; White, J. W. *J. Phys. Chem. B* **1997**, *101*, 10094−10104.
(30) Cheng, C.-H.; Shantz, D. F. *J. Phys. Chem. B* **2005**, *109*, 7266−7274.
(31) Davis, T. M.; Drews, T. O.; Ramanan, H.; He, C.; Dong, J.; Schnablegger, H.; Katsoulakis, M. A.; Kokkoli, E.; McCormick, A. V.; Lee Penn, R.; Tsapatsis, M. *Nature Mater.* **2006**, *5*, 400−408.
(32) Hsu, C. Y.; Chiang, A. S. T.; Selvin, R.; Thompson, R. W. *J. Phys. Chem. B* **2005**, *109*, 18804−18814.
(33) Tsay, C. S.; Chiang, A. S. T. *Microporous Mesoporous Mater.* **1998**, *26*, 89−99.
(34) Rajagopalan, K.; Peters, A. W.; Edwards, G. C. *Appl. Catal.* **1986**, *23*, 69−99.
(35) Sugimoto, M.; Katsuno, H.; Takatsu, K.; Kawata, N. *Zeolites* **1987**, *7*, 503−507.
(36) Gilson, J. P.; Derouane, E. G. *J. Catal.* **1984**, *88*, 538−541.
(37) Handreck, G. P.; Smith, T. D. *J. Chem. Soc., Faraday Trans.* **1989**, *85*, 645−654.
(38) Namba, S.; Inaka, A.; Yashima, T. *Zeolites* **1986**, *6*.
(39) Suzuki, I.; Oki, S.; Namba, S. *J. Catal.* **1986**, *100*, 219−227.
(40) Corma, A.; Davis, M. E. *ChemPhysChem* **2004**, *5*, 304−313.
(41) Corma, A.; Diaz-Cabanas, M. J.; Fornes, V. *Angew. Chem., Int. Ed.* **2000**, *39*, 2346−2349.
(42) Corma, A.; Diaz-Cabanas, M. J.; Garcia, H.; Palomares, E. *Chem. Commun.* **2001**, 2148−2149.
(43) Corma, A.; Rey, F.; Valencia, S.; Jorda, J. L.; Rius, J. *Nature Mater.* **2003**, *2*, 493−497.
(44) Corma, A.; Diaz-Cabanas, M. J.; Rey, F. *Chem. Commun.* **2003**, 1050−1051.
(45) Corma, A.; Puche, M.; Rey, F.; Sankar, G.; Teat, S. J. *Angew. Chem., Int. Ed.* **2003**, *42*, 1156−1160.
(46) Corma, A. *Stud. Surf. Sci. Catal.* **2004**, *154*, 25−38.
(47) Blasco, T.; Corma, A.; Diaz-Cabanas, M. J.; Rey, F.; Vidal-Moya, J. A.; Zicovich-Wilson, C. M. *J. Phys. Chem. B* **2002**, *106*, 2634−2642.
(48) Sastre, G.; Pulido, A.; Castaneda, R.; Corma, A. *J. Phys. Chem. B* **2004**, *108*, 8830−8835.
(49) Sastre, G.; Vidal-Moya, J. A.; Blasco, T.; Rius, J.; Jorda, J. L.; Navarro, M. T.; Rey, F.; Corma, A. *Angew. Chem., Int. Ed.* **2002**, *41*, 4722−4726.
(50) Gregg, S. J.; Sing, K. S. W. *Adsorption, Surface Area and Porosity*; Academic Press: London, UK, 1982.
(51) Rouquerol, F.; Rouquerol, J.; Sing, K. *Adsorption by Powders and Porous Solids*; Academic Press: London, UK, 1999.
(52) Glatter, O. *J. Appl. Crystallogr.* **1977**, *10*, 415−421.
(53) Glatter, O. *J. Appl. Crystallogr.* **1979**, *12*, 166−173.
(54) Glatter, O. *J. Appl. Crystallogr.* **1980**, *13*, 7−11.
(55) Glatter, O. *J. Appl. Crystallogr.* **1980**, *13*, 577−584.
(56) Glatter, O.; Kratky, O. *Small Angle X-ray Scattering*; Academic Press: London, UK, 1982.
(57) Svergun, D. I. *J. Appl. Crystallogr.* **1992**, *25*, 495−503.
(58) Guinier, A.; Fournet, G. *Small-Angle Scattering of X-rays*; John Wiley & Sons: New York, 1955.
(59) Kosslick, H.; Tuan, V. A.; Fricke, R.; Peuker, C.; Pilz, W.; Storek, W. *J. Phys. Chem.* **1993**, *97*, 5678−5684.
(60) van de Water, L. G. A.; van der Waal, J. C.; Jansen, J. C.; Cadoni, M.; Marchese, L.; Maschmeyer, T. *J. Phys. Chem. B* **2003**, *107*, 10423−10430.
(61) Lopez, A.; Soulard, M.; Guth, J. L. *Zeolites* **1990**, *10*, 134−136.
(62) Hay, D. G.; Jaeger, H. *J. Chem. Soc., Chem. Commun.* **1984**, 1433−1433.
(63) van de Water, L. G. A.; Zwijnenburg, M. A.; Sloof, W. G.; van der Waal, J. C.; Jansen, J. C.; Maschmeyer, T. *ChemPhysChem* **2004**, *5*, 1328−1335.
(64) Tuilier, M. H.; Lopez, A.; Guth, J. L.; Kessler, H. *Zeolites* **1991**, *11*, 662−665.
(65) Gabelica, Z.; Guth, J. L. *Angew. Chem., Int. Ed. Engl.* **1989**, *28*, 81−83.
(66) Fricke, R.; Kosslick, H.; Tuan, V. A.; Grohmann, I.; Pilz, W.; Storek, W.; Walther, G. *Stud. Surf. Sci. Catal.* **1994**, *83*, 57−66.
(67) Chou, Y. H.; Cundy, C. S.; Garforth, A. A.; Zholobenko, V. L. *Microporous Mesoporous Mater.* **2006**, *89*, 78−87.
(68) Li, Q.; Mihailova, B.; Creaser, D.; Sterte, J. *Microporous Mesoporous Mater.* **2000**, *40*, 53−62.
(69) Cheng, C.-H.; Shantz, D. F. *J. Phys. Chem. B* **2006**, *110*, 313−318.
(70) Yang, S.; Navrotsky, A.; Wesolowski, D.; Pople, J. A. *Chem. Mater.* **2004**, *16*, 210−219.
(71) Nikolakis, V.; Kokkoli, E.; Tirrell, M.; Tsapatsis, M.; Vlachos, D. G. *Chem. Mater.* **2000**, *12*, 845−853.
(72) Camblor, M. A.; Villaescusa, L. A.; Díaz-Cabañas, M. J. *Top. Catal.* **1999**, *9*, 59−76.
(73) Baes, C. F., Jr.; Mesmer, R. E. *The Hydrolysis of Cations*; John Wiley & Sons: New York, 1976.
(74) Knight, C. T. G.; Kirkpartrick, R. J.; Oldfield, E. *J. Am. Chem. Soc.* **1986**, *108*, 30−33.
(75) Knight, C. T. G.; Kirkpartrick, R. J.; Oldfield, E. *J. Am. Chem. Soc.* **1987**, *109*, 1632−1635.